Rev.Adv.Mater.Sci. 7 (2004) 32-40

A REAL TIME SCALE MEASUREMENT OF RESIDUAL STRESS EVOLUTION DURING COATING DEPOSITION USING ELECTRIC EXTENSOMETRY

J. O. Carneiro[1], V. Teixeira[1], A. Portinha[1], F. Vaz[1] and J.A. Ferreira[2]

[1]University of Minho, Physics Department, GRF Group, Azurém Campus, 4800-058, Guimarães, Portugal
[2]University of Minho, Physics Department, FAMO Group, Gualtar Campus, 4710-057, Braga, Portugal

Received: April 05, 2004

Abstract*:* High macroscopic residual stresses in thin coatings deposited by DC magnetron sputtering (MS) are caused by both the thermoelastic effects - thermal stress, and intrinsic stress, generated by high energetic particle bombardment during the coating deposition. In order to establish an alternative method for the study and characterization of the stress magnitude in a given coating/substrate system, this work reports an experimental technique, the *electric strain extensometry* (ESE), which is suggested to obtain the coating in-plane residual stresses level in a real time scale. A sensitivity analysis for *in situ* residual stress analysis was performed using a single active strain-gage sensor mounted in an arm of a Wheatstone bridge electric circuit. Two different coating/substrate systems - the molybdenum/glass and zirconium oxide/Ni-alloy composites – were prepared by DC magnetron sputtering (MS). The residual stress values developed in both systems were used to evaluate the electrical signal magnitude that would be obtained within ESE measurements. The predicted values fit well the experimental data, moreover, being in a range of several micro-Volts, they are quite detectable by a data acquisition system.

1. INTRODUCTION

Physical Vapour Deposition (PVD) processes, in particular, magnetron sputtering, have been shown to be powerful method for the synthesis of thin films with nanoscaled coating architecture - multilayered, nanocomposite, and nanostructured systems [1].

The major problems arising in PVD coating techniques during the production of fully prime reliant coatings are the understanding and modelling of the residual stresses which influence the mechanical integrity of PVD coatings through failure mechanisms. Another task is to verify the developed life prediction models by testing and, ultimately, to predict real component performance [2,3]. To study the coating stress generation mechanisms and to validate numerical models for residual stress analysis both *ex-situ* and *in-situ* stress measurement should be employed. The evaluation of the residual stresses developed in a coating/substrate system in a real time scale brings some additional advantages. They refer mainly to the quality control, since the *in-situ* residual stress time history evaluation (*via* the measurement of the strain field) permits a better adjustment of the deposition parameters and, in turn, the production of systems with improved mechanical quality and smaller rejection rates.

It is well-known that the mechanical and tribological properties of coated components depend mainly on the magnitude and the distribution of the residual stresses. Firstly, residual stress may cause the coating fracture and can also influence other coating properties like the wear resistance, corrosion resistance, *etc.* Secondly, the residual coating stress, together with chemical bonding, determines the adherence of the coating [2-5]. The dominating stress components are intrinsic stress related with

Corresponding author: J. O. Carneiro; e-mail: carneiro@fisica.uminho.pt

the coating grown-in defects, generated during coating deposition due to the high energetic particle bombardment, chemical reactions, and phase transformation and a thermal stress component due to a mismatch between the thermal expansion coefficients (CTE's) of substrate and coating [2,6].

Owing to the CTE and/or temperature gradients, residual stress develops in the coating-substrate structure which can cause delamination or fracture of the layer [2,3,7].

Far from the edges, the in-plane stress is typically compressive in ceramic coatings; large shear and normal stresses are generated at the free edge. Edge stresses are typically tensile within the ceramic and tend to promote crack propagation in the regions parallel and adjacent to the interface [3,8]. Therefore, cracking in the ceramic will affect the thermo-mechanical integrity of the functional coated component.

The tensile thermal coating stress becomes important at high working temperatures due to the relatively low thermal expansion coefficient of the discussed materials. In particular, this problem is one of the key points in the advanced power engineering since the protective coating are widely used here due to their ability to improve the performance and efficiency [9-11]. Regarding to tribological applications, hard and super-hard coatings are used in high-speed cutting tools where nanocomposite multilayered structure solutions are used to enhance thermo-mechanical stability [12-14].

2. MECHANICAL EVALUATION OF THE RESIDUAL STRESSES IN THIN FILM/SUBSTRATE COATED SYSTEMS

The total stress, σ_{tot}, acting in a film is the result of three different contributions: (i) external stresses, σ_{ext}, which are due to external loading; (ii) thermal stresses, σ_{th}, due to the mismatch between the thermal expansion coefficients of both substrate and film material and (iii) intrinsic stresses, σ_i, related with the particular coating microstructure and therefore, with the type of bonding between the film and substrate, the bombardment by working and reactive gases during film growth, and the particular growing process itself [2,5,6].

$$\sigma_{tot} = \sigma_{ext} + \sigma_{th} + \sigma_i . \quad (1)$$

The thermal component, considering a biaxial in-plane stress state for a very low film/substrate thickness ratio can be estimated by:

$$\sigma_{th} = E_f(\alpha_f - \alpha_s)(T_S - T_M). \quad (2)$$

where T_S is the coating temperature during the deposition process, and T_M is the ambient temperature (e.g, the temperature of the film/substrate coating after cooling) or the temperature at which the thermal stresses are determined, and E_f is the film elastic modulus, while α_f and α_s represent the thermal expansion coefficients of film and substrate, respectively. If no external load is applied, the sum of σ_{th} and σ_i can be considered as the temperature-dependent residual stress, $\sigma_r(T)$:

$$\sigma_r(T) = \sigma_{th} + \sigma_i . \quad (3)$$

The details of the stress distribution in a coating/substrate system can be very complex; however, some useful generalizations can be made. Fig. 1 shows an idealised representation of the in-plane normal stresses across the cross-section of a thin film and free-standing substrate at a point away from the edge. The stress distribution is determined by the requirement that the sum of the normal forces and bending moments (M_f and M_s for the film and substrate, respectively) over the total cross-section have to be zero [2,15,16]. Thus, stresses must reverse sign at the coating/substrate interface.

Assuming a biaxial plane stress field ($\sigma_{xx} = \sigma_{yy} = \sigma$; $\sigma_{zz} = 0$), the application of the generalised Hook's low enables to write for the substrate stress field, σ_s [16]

$$\sigma_s = \frac{E_s}{1-\nu_s}\varepsilon_s(z), \quad (4)$$

where E_s is the substrate elastic modulus, ν_s is the substrate Poison's modulus, and $\varepsilon_s(z)$ is the substrate elastic strain which depends on the distance z from the neutral plane to the considered substrate fibre. In order to balance the bending moment which is produced by the stressed film the substrate must bend. From classic theory of material mechanics, the substrate deflects with a constant curvature, *k,* produced by a pure bending moment. The elastic substrate strain field is given by [16,17]

$$\varepsilon_s(z) = zk. \quad (5)$$

The maximum elastic substrate strain ε_s occurs in the zones located far away from the neutral plane (i.e. $z_{max} = \pm t_s/2$), where t_s is the substrate thickness according Fig.1. The balance of both bending moments allows obtaining the film residual stress equation, σ_f (the so-called Stoney's equation) [18] where the film thickness is assumed to be much

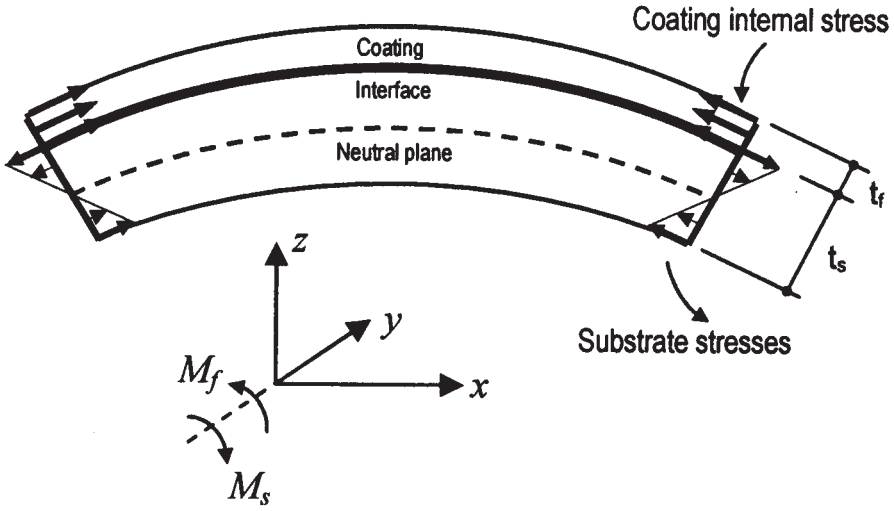

Fig. 1. Schematic representation of the stress distribution on coating and substrate cross-section.

smaller than the substrate thickness; using Eq. (5) σ_f can be written as a function of the substrate strain field, ε_s as

$$\sigma_f = \frac{E_s}{3(1-\nu_s)} \cdot \frac{t_s}{t_r} \varepsilon_s . \quad (6)$$

The substrate strain field, ε_s can be measured experimentally at each time moment of the deposition process using the electric extensometry technique. The basic theoretical aspects of the technique are described below.

3. THE STRAIN GAGE

When external forces are applied to a stationary object, stress and strain are the result. Strain is defined as the amount of deformation per unit length of an object when a load is applied. Strain may be compressive or tensile and is typically measured by strain gages. It was Lord Kelvin who first reported in 1856 that metallic conductors subjected to mechanical strain exhibit a change in their electrical resistance. This phenomenon was first put to practical use in the 1930s. Fundamentally, all strain gages are designed to convert mechanical motion into an electronic signal. The most widely used characteristic that varies in proportion to strain is electrical resistance. The first bonded, metallic wire-type strain gage was developed in 1938. The metallic foil-type strain gage (see Fig. 2) consists of a grid of wire filament (a resistor) of ~ 0.025 mm thickness, bonded directly to the strained surface by a thin layer of epoxy resin. When a load is applied to the surface, the resulting change in surface length is communicated to the resistor and the corresponding strain is measured in terms of the electrical resistance of the foil wire, which varies linearly with strain. The foil diaphragm and the adhesive bonding agent must work together in transmitting the strain, while the adhesive must also serve as an electrical insulator between the foil grid and the surface. If a wire is held under tension, it gets slightly longer and its cross-sectional area is reduced. This changes its electric resistance *R* in proportion to the strain sensitivity of the wire's resistance. The ideal strain gage should be small in size and mass, low in cost, easily attached and highly sensitive to strain.

When the strain is introduced, the strain sensitivity, which is also called the gage factor (S_g), is given by [19]

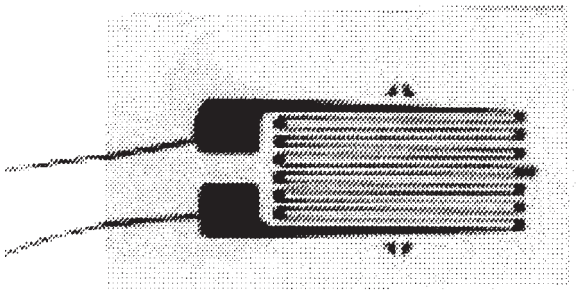

Fig. 2. Typical metal-foil strain gages.

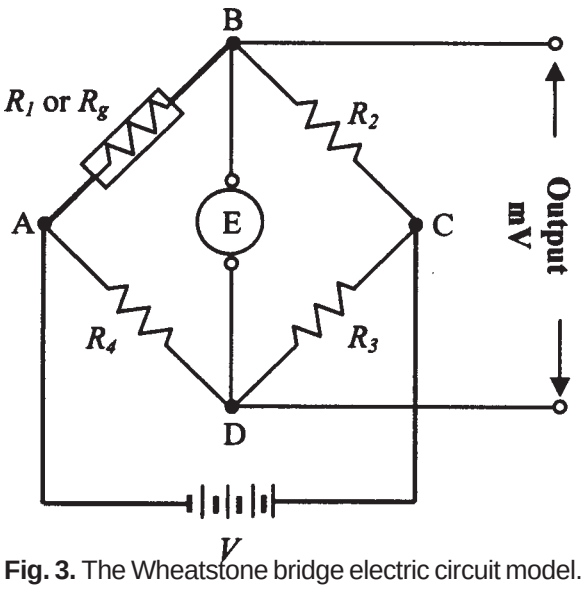

Fig. 3. The Wheatstone bridge electric circuit model.

$$S_g = \frac{1}{\varepsilon}\frac{\Delta R}{R}, \tag{7}$$

where ($\Delta R/R$) is the gage relative resistance change produced by the strained surface. Typical materials used for strain gage construction includes Constantan (copper-nickel alloy), Nichrome V (nickel-chrome alloy), platinum alloys (usually with tungsten), Isoelastic (nickel-iron alloy), or Karma-type alloy wires (nickel-chrome alloy) usually used for high temperatures applications. The most popular alloys used for strain gages are copper-nickel alloys and nickel-chrome alloys.

3.1. Strain- gage adhesives

The important stage of the strain gage mounting is a careful preparation of the substrate surface where the gage will be installed. It includes the elimination of oils, greases or any corrosion products in order to obtain a smooth and a polished surface. A wide variety of adhesives are available for bonding strain gages. The operating temperature is the main physical parameter that influences the selection of a specific adhesive. In order to operate at elevated temperatures, the stain-gage must be bounded using a *ceramic adhesive* because the organic adhesives cannot be employed here. Usually, the process uses ceramic powders such as alumina and silica combined with a phosphoric acid solution. A pre-coat of the ceramic cement is applied and fired to form an insulation thin layer between the gage grid and the substrate. One of the commercial cements, identified as NBS-x-142, is usually recommended for high temperatures [20], since it shows a very high resistivity at temperatures up to 980 °C.

3.2. The Wheatstone bridge model

In order to measure strain with a bonded resistance strain gage, it must be connected to an electric circuit that is capable to measure the changes in resistance corresponding to a strain. A strain gage sensor is usually electrically connected [21,22] to form a Wheatstone bridge circuit (see Fig. 3). A Wheatstone bridge is a divided bridge circuit used for the measurement of static or dynamic electrical resistance. The output voltage of the Wheatstone bridge is usually expressed in millivolts output per volt input.

The electric circuit is normally employed with the active strain gage(s) constituting one, two, or all four arms of the bridge (quarter-, half-, or full-active bridge). Let us consider the circuit shown in Fig. 3 to illustrate the principle of the Wheatstone bridge circuit operation.

If the resistive elements R1, R2, R3, and R4 are equal (see Fig. 3), and a voltage, *V*, is applied between points A and C, then the output between points B and D will show no potential difference. However, if R1 is changed to some value which is not equal to R2, R3, and R4, the bridge will become unbalanced and a voltage will arise at the output terminals. In a so-called G-bridge configuration, the variable strain sensor has a resistance *Rg*, while the other arms are fixed value resistors. The sensor, however, can occupy one, two, or four arms of the bridge, depending on the application. The total strain or output voltage of the circuit *E* is equivalent to the difference between the voltage drop across R1 or Rg and R4. This can also be written as:

$$E = V_{BD} = (V_{AB} - V_{AD}) \tag{8-a}$$

or

$$E = \frac{R_1R_3 - R_2R_4}{(R_1 + R_2)(R_3 + R_4)}V. \tag{8-b}$$

The bridge is considered balanced [23] when $R_1 \cdot R_3 = R_2 \cdot R_4$ and, therefore, *E* equals zero. Any small change in the resistance of the sensing grid will throw the bridge out of balance, making it suitable for the detection of strain. When the bridge is set up so that *Rg* is the only active strain gage, a small change in *Rg* will result in an output voltage from the bridge. The bridge voltage output *E*, can be ob-

tained from Eq. (8b) and for the assembly of 1/4 of the bridge (only one active gage is set up, outer resistances have the nominal values equal to the active gage resistance, see Fig. 4) it becomes

$$\frac{E}{V} = \frac{S_g \varepsilon \cdot 10^3}{4} \tag{9}$$

with (*E/V*) expressed in millivolts per volt input. So the experimental strain is given by

$$\varepsilon = \frac{4 \cdot 10^{-3}}{S_g} \cdot \frac{E}{V}. \tag{10}$$

Thus, from the above considerations, it is now possible to evaluate the intrinsic residual stress component on a coatings/substrate system in a real time scale *via* the measuring of the output voltage from the Wheatstone bridge. In fact, substituting Eq. (10) into Eq. (6) Stoney's equation can now be re-written as

$$\sigma_f = \frac{4 \cdot 10^{-3}}{3} \frac{E_s}{(1-\nu)} \frac{t_s}{t_f} \frac{1}{S_g} \frac{E}{V}. \tag{11}$$

Considering Eqs. (2) and (3) one should expect that the stresses observed in two different substrates with different thermal expansion coefficients must be equal if the contributions of σ_{th} and σ_{ext} equals zero. This assumption is true if the temperature at which the thermal stresses component is determined, T_M, becomes equal to the substrate temperature, T_s, during coating deposition. Actually, during coating deposition, the strain gage, being mounted under the substrate, is able to evaluate the intrinsic strain field continuously [using Eq. (11)]; the gage is evaluating the intrinsic film stress component, σ_i here because T_M is equal to T_s. After coating deposition, the thermal stress component due to film/substrate cooling can be determined from Eq. (3). In this case, the total residual stress $\sigma_r(T)$ is measured by the strain gage and the thermal stress component is obtained from the subtraction between $\sigma_r(T)$ and σ_i.

4. SENSITIVITY ANALYSIS: OUTPUT VOLTAGE EVALUATION FROM EXPERIMENTAL RESULTS OF SPUTTERED COATINGS

In order to evaluate the time dependence of the output voltage during the MS deposition process, two kinds of experimental results related with intrinsic stress were used in this work in accordance with

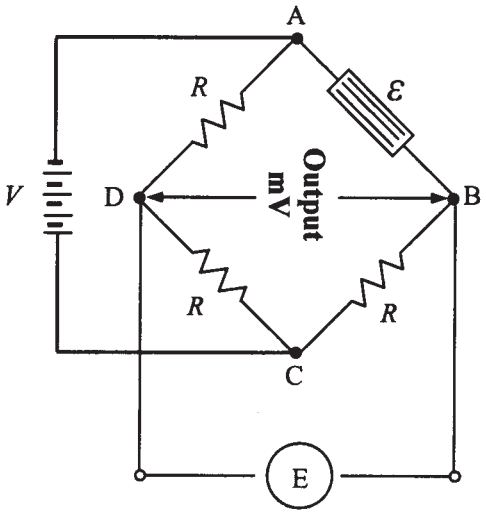

Fig. 4. Assembly in 1/4 of bridge; single active gage in any strain field.

Teixeira *et al.* [24,25]. The first kind of results is related to the deposition of a thin molybdenum film on a glass substrate. Molybdenum (Mo) is a refractory metallic element used principally as an alloying agent in steel, cast iron, and superalloys to enhance hardness, strength, toughness, and wear and corrosion resistance. The metal is also used in nuclear energy applications and for missile and aircraft parts. Thin films of refractory metals such as molybdenum are frequently used in several technological applications going from metallization in integrated circuits for electronic components up to mechanical components, where the application of a protective coating is a more and more common practice in order to improve the tribological performances. The second kind of results is related to the deposition of a thin zirconium oxide film stabilized with ytrium oxide (ZrO_2-Y_2O_3) on a Ni-alloy substrate (Inconel 600).

Pure Zirconia (ZrO_2) has a high melting point (2700 °C) and a low thermal conductivity. Its polymorphism, however, restricts its widespread use in ceramic industry. During a heating process, zirconia will undergo a phase transformation process. The change in volume associated with this transformation makes the usage of pure zirconia in many applications impossible. Addition of some oxides (Y_2O_3, MgO and Al_2O_3 into the zirconia structure results in a solid solution with a cubic structure; this solution has no phase transformation during heating and cooling. Reactive DC magnetron sputtering allows to produce totally or partially stabi-

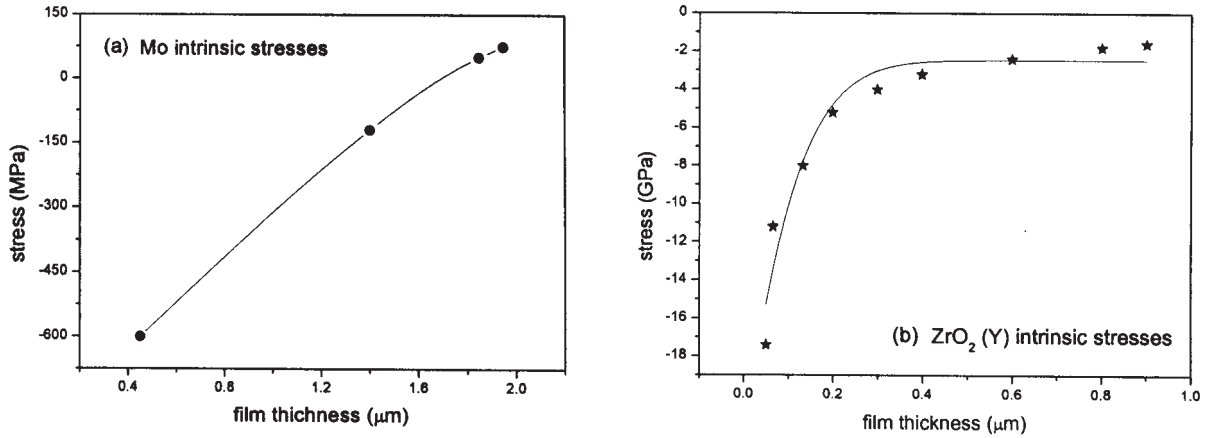

Fig. 5. Intrinsic stress as a function of the coating thickness (a) Molybdenum (b) Zirconia.

lized ZrO_2 coatings with a well defined portion of stabilizing agent, whereby the authors concentrated on the system ZrO_2 - Y_2O_3 in this work. Depending on deposition conditions of the sputtered process, ZrO_2 (Y) coatings deposited by MS may be relatively dense and in a controlled state of compressive stress at room temperature.

Details of the coatings preparation, DC magnetron sputtering hardware and characterisation are described elsewhere [24-26]. For both experiments, the *in situ* residual stress measurements of the deposited coatings showed the expected bending on the coating/substrate system. For the molybdenum coating, the deposition was carried out in an Ar atmosphere. A pure metallic Mo target with a 0.01 m^2 area and a $24 \times 24 \times 0.15$ mm^3 glass substrate were used in the runs. For the stabilized zirconia coating an Inconel 600 substrate ($70 \times 20 \times 0.6$ mm^3), was used and the deposition was carried out in an Ar/O_2 atmosphere. For both coating/substrate systems, a summary of the deposition parameters as well as the thermoelastic properties (elastic modulus *E*, Poisson ratio ν, and thermal expansion coefficient, α) are shown in Tables 1 and 2, respectively.

Fig. 5 demonstrates the intrinsic stresses evolution, σ_i as a function of the coating thickness for molybdenum and stabilized zirconia coatings. For both cases, the intrinsic compressive stresses decrease with thickness increase. These results are consistent with the theory [4,8] stating that thinner coatings should have higher compressive stresses. An increase in the coating thickness eventually moves the coating stress to a tensile state (which occurs in the molybdenum film); this fact can be explained as being due to the growth of the film with a columnar structure. Actually, an increase in the column height makes higher the probability of the column collapse; for this reason, it promotes film relaxation and a concomitant decrease in the compression stress field [2,15].

Table 1. Summary of MS deposition parameters for molybdenum and zirconia coatings.

Deposition Parameters	Molybdenum	Zirconia
Substrate temperature	135 ºC	160 ºC
Target/substrate distance	50 mm	82 mm
Sputter current	0.25 A	1 A
DC substrate polarization	-100 V	-50 V
Base pressure	$1.5 \cdot 10^{-3}$ Pa	$1.3 \cdot 10^{-3}$ Pa
Sputter gas pressure (Ar)	$2.0 \cdot 10^{-3}$ mbar	$6.4 \cdot 10^{-3}$ mbar
O_2 reactive gas pressure	–	$1.4 \cdot 10^{-4}$ mbar
Deposition rate, *r*	3.6 μm/h	0.72 μm/h

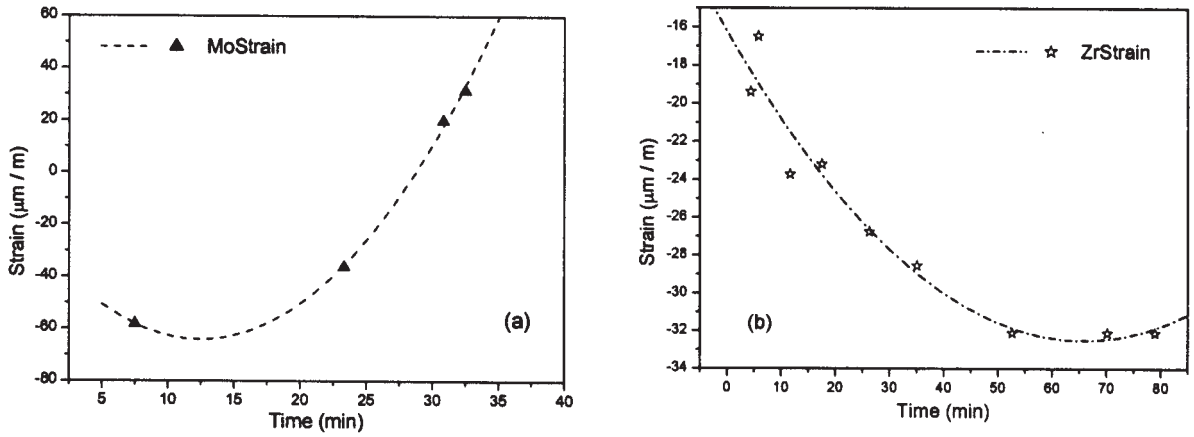

Fig. 6. Coating strain field as a function of the deposition time (a) molybdenum and (b) zirconia.

The intrinsic stress in the Mo-coatings varies from strongly compressive for very low sputtering gas pressures to highly tensile at intermediate gas pressure and slightly compressive at high gas pressures [27]. Several mechanisms have been suggested in the literature which may explain this variation. We consider the low level of the energetic particle bombardment typical for high sputter gas pressure as a key factor for the stress development, because voids and spaces between grains remain in the coating [2].

Zirconia exhibits phase transformation from monoclinic to a tetragonal structure at ~1150 °C and from tetragonal to a cubic at ~2400 °C. As referred, this phase transformations are accompanied by important volume changes and damage due to the resulting stress in the coating. The zirconia coatings studied were therefore stabilized by Y_2O_3 (5-7 wt.%) to suppress this phase transformations[28]. The intrinsic stress in zirconia coating is always compressive, but it diminishes with augmenting film thickness. At about 2 GPa, the stress level maintains approximately the same with increasing film thickness (see Fig. 5b). This behaviour is well known and can be understood qualitatively on the basis of the grain boundary relaxation model by Hoffman [29,30].

The electric output voltage and coating strain time evolution during the deposition process were predicted *via* Eqs. (10) and (11) where a linear time dependence was assumed for the coating thickness (i.e. $t_f = rt$) where r is the deposition ratio. Fig. 6 shows the strain evolution of the molybdenum and zirconia coatings as a function of the deposition time. As seen from the figure, the strain changed from compressive to moderate tensile for the molybdenum coating and from slightly compressive to moderate compressive for the zirconia coating. So the tensile strain in the Mo coating can be attributed to the interatomic forces between adjacent columns. When the sputter gas pressure decreases, the tensile strain (and, concomitantly, the stress) in the coating increases due to the fact that the gaps between columns became closed [27]. For zirconia coating, the strain is always compressive, but maintains approximately the same with increasing film thickness (see Fig. 6b). Emphasize that this behaviour can be understood qualitatively on the basis of the grain boundary relaxation model by Hoffman.

This behaviour manifest itself in the values of the output electrical voltage values, which are presented in Table 3 for both molybdenum and zirconia coatings at different time moment of the coating deposition. It is seen from the table that the electrical output voltage values are in order of several micro-Volts, enabling a significant sensitivity for small changes of curvature during coating deposition. This allows us to study the stress relaxation (see Fig. 5a) as

Table 2. Thermo/elastic parameters for the substrate and coating materials.

	Thermo / Elastic Properties		
Material	E (GPa)	ν	$\alpha \cdot 10^{-6}$ (K^{-1})
Glass	65	0.3	3.2
Molybdenum	275.9	0.32	5.4
Inconel 600	200	0.3	15
Zirconia	170	0.23	10

Table 3. Output voltage data as a function of the coating deposition time for molybdenum and zirconia.

Coating material	Time (min)	Output Voltage (μV/V)
Molybdenum	7.5	-29.6
	23.3	-18.1
	30.8	9.96
	32.5	15.8
Zirconia	4.4	-9.7
	17.5	-11.6
	25.2	-13.2
	35.0	-14.3
	52.6	-16.1
	77.0	-16.02

well as the increase of compressive stress due to high energetic particle bombardment (see Fig. 5b).

As was referred, the strain gage is designed to transmit effectively the surface strain to the sensing grid. For the case of a single active gage layout (see Fig. 4) having a gage factor of 2, the output from the unbalanced Wheatstone bridge is 1/2 mV/V for each unit of $\mu\epsilon$. For most practical applications, bridge excitation, *V* is limited to a range of 1 to 20 volts with lower voltages being more common.

For a bridge excitation of 5 volts, the bridge output is 2.5 μV per $\mu\epsilon$. This is the magnitude of signal which is resolved with a strain measuring system with a sensitivity of 1 $\mu\epsilon$. Signals from strain gage bridges are usually very small and require significant amplification if the strain measuring system requires a sensitivity of resolving 1 $\mu\epsilon$. The instrumentation requirements for such measurements with strain gages are quite more complex than those for a simple amplifying of the signal from a Wheatstone bridge. It should include a stable power supply for the bridge (more usually, constant voltage) and precision resistors for any active arm of the bridge. As a result, the amplifiers which are commonly used in commercial strain-gage instrumentation have gains of up to 1000. If the strain data is acquired as $\mu\epsilon$ signals, the selection of an analog-to-digital convertor (ADC) hardware is determined by the required measurement range. Thus, a 14-bit ADC can be used since it covers a strain range of ± 16384 $\mu\epsilon$ that is suitable for most applications.

5. CONCLUSIONS

From the above case studies, it was demonstrated that it is possible to evaluate indirectly the intrinsic residual strain and stress evolution during coating deposition *via* the measurement of the electric output voltage from the unbalanced Wheatstone bridge. From the numerical calculations of residual stresses in a coating/substrate system, the following conclusions can be highlighted: *(i)* both analysed coating/substrate systems have generated residual stresses during the coating deposition. The magnitude of the residual stresses has changed with the increase in the film thickness. The residual stress values were used to achieve the sensitivity of the electrical signal (electric output voltage from the unbalanced Wheatstone bridge) which are suitable for the accurate ESE measurements both systems; *(ii)* it was possible to evaluate the residual strains on a coating/substrate system in a real time scale using the modified Stoney equation by measuring the electric output voltage. The predicted values, being in a range of some micro-Volt, were quite detectable by a data acquisition system; *(iii)* the proposed alternative, *in-situ* and real time scale measurement method, allows a reliable and efficient evaluation of the residual stresses evolution in sputtered coatings, and thus contributing to a detailed study of the coating stress generation mechanisms and to validate numerical models for PVD coatings. The information gained from *in situ* stress measurements allows to separate thermal and intrinsic stresses.

ACKNOWLEDGEMENTS

The authors should like to address a special thank to *Agostinho Magalhães Gomes*, a Mechanical Engineering student which has made with patience all the drawings for this work.

REFERENCES

[1] A. Portinha, V. Teixeira, J. Carneiro, S.N. Dub and R. Shmegera // *Rev. Adv. Mat. S*ci. **5** (2003) 34.

[2] M. Ohring, *The Materials Science of Thin Films* (Academic Press, San Diego, USA, 1992)

[3] M. D. Thouless // *J. Vac. Sci. Technol.* **A(9)** (1991) 2510.

[4] V. Teixeira // *Thin Solid Films* **392** (2001) 276.

[5] F. Vaz, L. Rebouta, P. Goudeau, J. P. Riviére, M. Bodmann, G. Kleer and W. Döll // *Thin Solid Films* **402** (2002) 195.

[6] J. A. Thornton and D. W. Hoffman // *Thin Solid Films* **171** (1989) 5.
[7] U. Marewski, D. Stöver and R. Hecker // *Surface and Coatings Technology* **46** (1991) 47.
[8] J. A. Thornton and D. W. Hoffman // *J. Vac. Sci. Technol.* **A(4)** (1986) 3059.
[9] V. Teixeira, M. Andritschky, W. Fischer, H. P. Buchkremer and D. Stöver // *Surface and Coatings Technology* **120-121** (1999) 103.
[10] M. Alaya, G. Grathwohl and J. Musil, In: *Proc. 3rd Int. Symp. on Sructural and Functional Gradient Materials*, ed. by Ilschner and Cherradi (Switzerland, 1994) p. 405.
[11] Vasco Teixeira, In: *Nanostructured Materials and Coatings for Biomedical and Sensor Applications*, ed. Y.G. Gogotsi and I.V. Uvarova (Kluwer Academic Publishers, 2003) p. 131.
[12] C. J. Tavares, L. Rebouta, J. P. Riviére, J. Pacaud, H. Garem, K. Pischow and Z. Wang // *Thin Solid Films* **398-399** (2001) 397.
[13] F. Vaz, L. Rebouta, P. Goudeau, J. Pacaud, H. Garem, J. P. Rivičre, A. Cavaleiro and E. Alves // *Surf. Coat. Technol.* **133-134** (2000) 307.
[14] E. Ribeiro, A. Malczyk, S. Carvalho, L. Rebouta, J. V. Fernandes, E. Alves and A. S. Miranda // *Surf. Coat. Technol.* **151-152** (2002) 515.
[15] J. A. Thornton // *Ann. Rev. Mater. Sci.* **7** (1977) 239.
[16] S.P. Timoshenko and J.N. Goodier, *Theory of Elasticity* (McGraw-Hill Inc., Tokyo, 1970).
[17] J.M. Alexander, *Strength of Materials, Vol. I* (Ellis Hordood Ltd, Chicherter,UK, 1981).
[18] G.G. Stoney // *Proc. R. Soc. (Lond.)* **A 82** (1909) 172.
[19] L.D. Lineback, *Strain Gage meets Computer in the Teaching Laboratory* (*Measurements Group*, Inc. Raleigh, North Carolina, USA, 1985).
[20] J.M. Dally and W.F. Riley, *Experimental Stress Analysis* (McGraw-Hill Book Co. – Singapore, 1991).
[21] C.C. Perry and H.R. Lissner, *The Strain Gage Primer, 2nd ed.* (McGraw-Hill Book Co. - New York, 1982).
[22] *Strain Gage Technology*, ed by. A.L. Window and G.S. Holister (Applied Science Publishers, 1982).
[23] P. Horowitz and W. Hill, *The Art of Electronics*, *2nd ed.* (Cambridge University Press, New York, 1989).
[24] M. Andritschky and V. Teixeira // *Vacuum* **43** (1992) 455.
[25] M. Andritschky and V. Teixeira // *Vacuum* **45** (1993) 1047.
[26] J. B. Almeida // *Vacuum* **39** (1989) 717.
[27] V. Teixeira and M. Andritschky // *NATO Series e-Appl. Sci* (Kluwer Ac. Publ.,) Vol. **234** (1992) 121.
[28] S.B. Qadri, C. M. Gilmore, C. Quinn, E. F. Skelton, C. R. Gosset // *J. Vac. Sci. Technol*. **A7 (3)** (1989) 1220-1224.
[29] R.W. Hoffman, In: *Physics of Thin Films*, *Vol 3*, ed. by G. Haas and R. Thun, (Academic Press, New York, 1966) p. 211.
[30] F.A. Doljack and R.W. Hoffman // *Thin Solid Films* **12** (1972) 71.